Experimental Frequency-Domain Analysis of Nonlinear Controlled Optical Storage Drives

Marcel Heertjes, Erik Pastink, Nathan van de Wouw, and Henk Nijmeijer, *Fellow, IEEE*

***Abstract*—For nonlinear controlled optical storage drives, a frequency-domain measurement approach is shown to be effective in demonstrating both stability and performance. In an experimental setting based on an industrial optical playback (CD drive) device, the motivation for applying such an approach is illuminated. It is shown that performance can efficiently be assessed using a describing function approach on a model level and using swept-sine measurements on an experimental level. The validity and effectiveness of the approach is extensively shown via closed-loop measurements.**

***Index Terms*—Asymptotic stability, circle criterion, describing functions, feedback control, nonlinear systems, optical recording.**

I. Introduction

FROM the early introduction of CD applications in the 1980s to today's DVD applications, the servo control design of optical storage drives is mainly driven by linear control theory [12], [13]. For portable or automotive applications, this generally implies the following tradeoff: improved low-frequency disturbance rejection is obtained under decreased stability margins. Related to this fact, improved (low-frequency) shock suppression in view of road excitation or engine vibrations is balanced by the performance decrease under (high-frequency) disc defect disturbances like scratches, fingerprints, or dirt spots. In the broader sense of fundamental design limitations [4], this tradeoff is considered in the philosophy to apply nonlinear control for linear systems as a means to enhance performance beyond such limitations.

Nonlinear control, or more specifically, nonlinear proportional-integral-derivative (PID) control (see also the work of Armstrong *et al.* [1], Jiang and Gao [9], and Fromion and Scorletti [5]) combines the possibility of having increased performance in terms of shock attenuation without unnecessarily deteriorating the time response under disc defect disturbances. For this purpose, the integrator part of a nominal PID controller is given a variable gain wherein large levels of disturbance typically induce a more than proportional increase in the control action. As a result, large shocks and vibrations are more effectively handled than small shocks and vibrations.

Manuscript received January 10, 2005; revised June 3, 2005. Manuscript received in final form November 15, 2005. Recommended by Associate Editor D. W. Repperger.

M. Heertjes is with the Department of Mechatronics Technologies, Philips Applied Technologies, 5600 MD Eindhoven, The Netherlands (e-mail: marcel.heertjes@philips.com).

E. Pastink is with the Research and Development Department, Océ, 5900 MA Venlo, The Netherlands (e-mail: hp@oce.nl).

N. van de Wouw and H. Nijmeijer are with the Department of Mechanical Engineering, Eindhoven University of Technology, 5600 MB Eindhoven, The Netherlands (e-mail: n.v.d.wouw@tue.nl; h.nijmeijer@tue.nl).

Digital Object Identifier 10.1109/TCST.2005.863658

Contrary to previous experimental work [7] that merely considered nonlinear performance in terms of time-domain responses, this paper deals with an experimental performance analysis based on frequency-domain measurements. To this end, a combined describing function and swept-sine measurement approach is shown to offer both an efficient and sufficiently accurate tool for studying global qualitative nonlinear behavior. This is demonstrated on an industrial optical playback (CD drive) device. Not only does the approach efficiently reveal both the amplitude and frequency dependency under different levels of shocks and vibrations, but it also provides measured amplitude and phase characteristics. The latter, which is generally unavailable in nonlinear analysis, is of special interest, because of its relation with time-domain properties like damping that largely affect the system response under disc defect disturbances. In this respect, an efficient experimental analysis tool enhances the applicability of the nonlinear control design, which, by itself, provides a strong driver for its application.

This paper is organized as follows. In Section II, the nonlinear control design based on a simplified objective lens model is presented. This includes stability analysis in terms of absolute stability theory. In Section III, model validation is conducted using the proposed describing function and swept-sine frequency-domain measurement approach. In Section IV, this approach is used to assess nonlinear system performance. In Section V, the main conclusions regarding this paper are summarized.

II. Dynamics, Measurement, and Control of Optical Storage Drives

The application of a nonlinear PID control strategy is experimentally studied on an optical playback (CD drive) device. To this end, first, the CD drive test setup is presented; second, the principles of optical storage are briefly discussed; third, a model is given for the nonlinearly controlled objective lens dynamics in so-called radial direction; and fourth, the stability of the nonlinear controlled objective lens dynamics is assessed from an absolute stability standpoint.

The experimental setup is depicted in Fig. 1. It consists of an interface to flash source code into a microcontroller, an interface to adapt the controller parameters once flashed and to designate desired servo signals, an IO-board for monitoring these signals and providing the means to inject noise in the servo loop, a SigLab/MatLab combination for signal processing and generation, and naturally a CD drive mechanism. The microcontroller is freely programmable and supports a discrete representation of a user-defined controller given a sampling frequency of 90 kHz. For the purpose of system identification and measurement, several servo signals can be measured whereas an injection point is

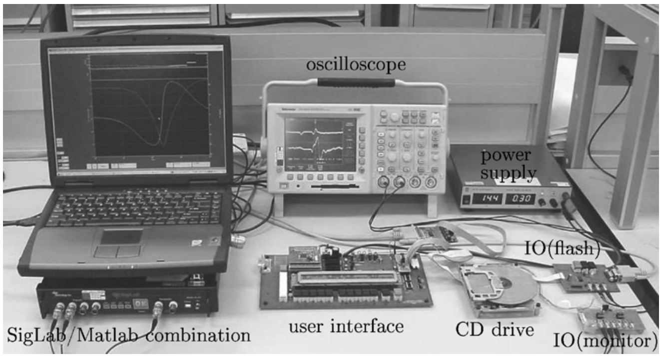

Fig. 1. CD drive test setup.

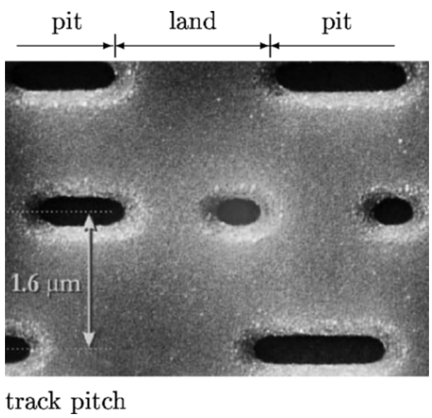

Fig. 2. Disc (CD) surface.

available for applying an additional voltage level over the servo motor coils, i.e., the actuators needed for position control.

The CD drive contains several actuators (motors) for control, not only to regulate the disc rotation speed needed to obtain a constant data rate along the disc radius but also to control an objective lens in following a desired disc track. The latter is done to enable reading information from the disc. Information on the disc is stored via a sequence of nonreflective pits separated by reflective lands; see Fig. 2. For a CD, pits typically have dimensions varying between 0.9 and 3.3 μm in length. The pit width equals 0.6 μm. To obtain data from the disc, the objective lens is controlled in two directions: the focus direction, i.e., perpendicular to the disc plane, and the radial direction, i.e., in the disc plane but perpendicular to the disc tracks. Herein the radial direction is of particular interest because of its sensitivity to external shocks and vibrations. This direction is studied under the assumption that the nonlinear control strategy could also be applied in the focus direction, hence the direction needed to focus a light spot on the disc information layer.

The closed-loop objective lens dynamics in the radial direction are depicted in Fig. 3 in block-diagram representation. Herein the radial position of the objective lens is represented by the output signal $y_{\rm r}$, whereas the radial disc track position is represented by the reference signal r. The radial error signal is given by $e_{\rm r} = r - y_{\rm r}$ and represents the only radial position signal readily available from measurement. For the purpose of measurement, an injection point is added for applying an injection signal i whereas two additional signals can be monitored: the controller output signal ${\rm o_c}$ and the process input signal ${\rm o_i}$.

The objective lens is modeled by a series connection of a second-order mass-spring-damper system, a first-order low-pass filter, and a two-sample time delay. This is given in transfer function notation by

$$\mathrm{P}(s) = \frac{y_{\rm r}}{\rm o_i}(s) = \underbrace{\frac{1}{\mathrm{m}s^2 + \mathrm{b}s + \mathrm{k}}}_{\text{mass−spring system}} \underbrace{\frac{\omega_{\rm lp,1}}{s + \omega_{\rm lp,1}}}_{\text{lowpass}} \underbrace{\exp(-T_{\rm d}s)}_{\text{time delay}} \quad (1)$$

with $s \in \mathbb{C}$ the Laplace variable. The first part of the model contains the lens unit mass $\mathrm{m} = 1.5 \times 10^{-4}$ kg together with the mechanical properties of the objective lens support, i.e., damping and stiffness properties $\mathrm{b} = 2.2 \times 10^{-2}\ \mathrm{Ns \cdot m^{-1}}$ and $\mathrm{k} = 21.3\ \mathrm{N \cdot m^{-1}}$, respectively. The second part of the model represents a first-order low-pass filter with a cutoff frequency of $\omega_{\rm lp,1} = 6.2 \times 10^4$ rad s^{-1}. This part is related to the actuator inductance in the transfer from voltage to current; see Bittanti *et al.* [2] for a similar physical model description. Based on a sampling frequency of $\mathrm{f_s} = 90$ kHz, a two-sample time delay with $T_{\rm d} = 2/\mathrm{f_s}$ is needed to take digital implementation issues into account.

For radial tracking, nominal servo control is based on a series connection of a PID-controller and a second-order low-pass filter. Its Laplace representation is given by the transfer function

$$\mathrm{C_1}(s) = \underbrace{\frac{\mathrm{k_p}\left(s^2 + (\omega_{\rm d} + \omega_{\rm lag})s + (1+\gamma)\omega_{\rm d}\omega_{\rm lag}\right)}{\omega_{\rm d}(s + \omega_{\rm lag})}}_{\text{pid}} \cdots \underbrace{\frac{\omega_{\rm lp,2}^2}{s^2 + 2\beta\omega_{\rm lp,2}s + \omega_{\rm lp,2}^2}}_{\text{lowpass}} \quad (2)$$

with $\mathrm{k_p} = 2.7 \times 10^3\ \mathrm{N \cdot m^{-1}}$ the radial loop gain, $\gamma = 20$ a dimensionless gain corresponding to a lag filter, $\omega_{\rm lag} = 8.4 \times 10^1$ rad s^{-1} the lag filter cutoff frequency, $\omega_{\rm d} = 1.9 \times 10^3$ rad s^{-1} the cutoff frequency of a lead filter, $\omega_{\rm lp,2} = 4.4 \times 10^4$ rad s^{-1} the cutoff frequency of the second-order low-pass filter, and $\beta = 1.1$ its dimensionless damping coefficient. To improve the (low-frequency) disturbance rejection but not deteriorate the (high-frequency) response to noise, an additional control contribution is considered, which consists of the following series connection of a notch filter, a PI filter, and a second-order low-pass filter

$$\mathrm{C_2}(s) = \underbrace{\frac{s^2 + 2\beta_1\omega_{\rm n}s + \omega_{\rm n}^2}{s^2 + 2\beta_2\omega_{\rm n}s + \omega_{\rm n}^2}}_{\text{notch}} \underbrace{\frac{\mathrm{k_p}\gamma\omega_{\rm lag}}{s + \omega_{\rm lag}}}_{\text{pi}} \underbrace{\frac{\omega_{\rm lp,2}^2}{s^2 + 2\beta\omega_{\rm lp,2}s + \omega_{\rm lp,2}^2}}_{\text{lowpass}} \quad (3)$$

with $\omega_{\rm n} = 1.8 \times 10^3$ rad s^{-1} the cutoff frequency of the notch filter and $\beta_1 = 0.2$, $\beta_2 = 4.1$ corresponding dimensionless damping coefficients. The overall controller can now be given by the transfer function

$$\mathrm{C}(s) = \frac{\rm o_c}{e_{\rm r}}(s) = \mathrm{C_1}(s) + \phi\mathrm{C_2}(s) \quad (4)$$

where $\phi > 0$ determines the contribution of $\mathrm{C_2}$.

The choice for ϕ comprises a performance tradeoff. Increasing its value induces improved (low-frequency) shock

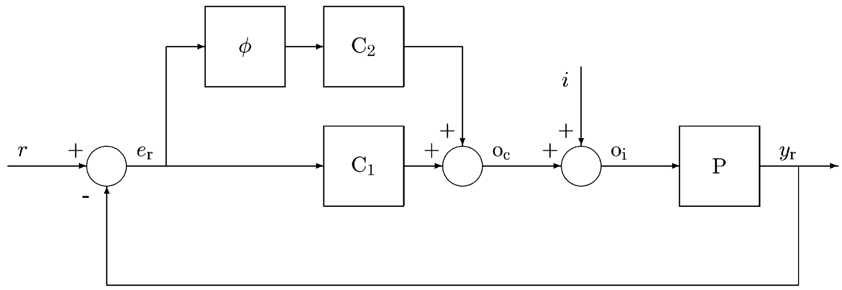

Fig. 3. Closed-loop objective lens dynamics in radial direction.

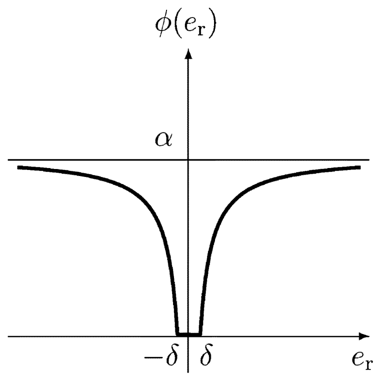

Fig. 4. Graphical representation of the nonlinear gain $\phi(e_\mathrm{r})$.

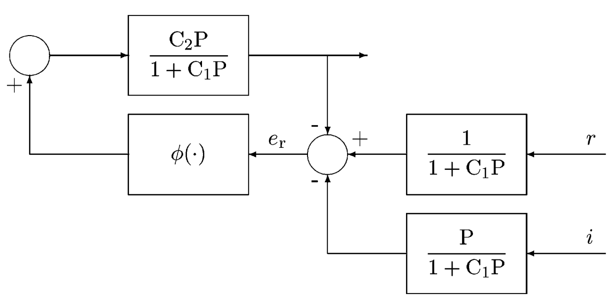

Fig. 5. Nonlinear closed-loop dynamics in absolute stability representation.

suppression, but with less phase margin. Subsequently, less phase margin negatively influences the step response under disc defect disturbances. To surpass this tradeoff, ϕ is given an input dependency defined (in time domain) by

$$\phi(e_\mathrm{r}) = \begin{cases} \alpha\epsilon(e_\mathrm{r}) - \frac{\delta}{|e_\mathrm{r}|}, & \text{if } |e_\mathrm{r}| \geq \delta \\ 0, & \text{if } |e_\mathrm{r}| < \delta \end{cases} \tag{5}$$

with

$$\epsilon(e_\mathrm{r}) = \begin{cases} 1, & \text{if } |e_\mathrm{r}| \geq \delta \\ 0, & \text{if } |e_\mathrm{r}| < \delta \end{cases} \tag{6}$$

where $\alpha > 0$ is a gain limit value and $\delta > 0$ is a deadzone length; see Fig. 4 for a graphical representation. For this choice of nonlinearity, the overall nonlinear PID control design is shown in Fig. 5 in so-called absolute stability representation, that is, a linear time-invariant system $\mathrm{C}_2/(1+\mathrm{C}_1\mathrm{P})$ in the feedback connection with a sector-bounded nonlinearity $\phi(e_\mathrm{r})$. Sector-boundedness immediately follows from

$$0 \leq \phi(e_\mathrm{r})e_\mathrm{r}^2 \leq \alpha e_\mathrm{r}^2 \tag{7}$$

with $\phi(e_\mathrm{r})$ being a positive semidefinite function; see also Fig. 4.

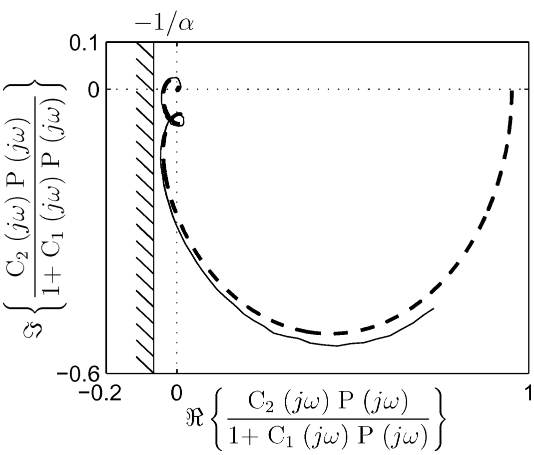

Fig. 6. Graphical interpretation of (8).

Stability of the nonlinear feedback connection can now be studied using absolute stability theory; see Brockett [3] for an introduction of formerly unknown Russian literature. For the considered class of systems, and given the considered system properties, finite gain $\mathcal{L}_2$ stability is guaranteed if the following frequency-domain inequality is satisfied:

$$\Re\left\{\frac{\mathrm{C}_2(j\omega)\mathrm{P}(j\omega)}{1+\mathrm{C}_1(j\omega)\mathrm{P}(j\omega)}\right\} > -\frac{1}{\alpha}, \quad \forall\omega \in \mathbb{R}. \tag{8}$$

Moreover for zero input, the origin $e_\mathrm{r} = 0$ can be made globally asymptotically stable. This is an application of the circle criterion; see [10] for a more detailed description regarding the conditions imposing stability. Equation (8) allows for a graphical interpretation as shown in Fig. 6. It follows that stability is guaranteed if the Nyquist curve remains to the right of a vertical line through the point $(-1/\alpha,0)$. Both in measurements (solid) and simulations (dashed), it can be seen that the curve satisfies this condition for $\alpha \leq 26$. It is important to realize that the choice of the notch filter parameters in (3) significantly contributes to the enlargement of the stability range; see Heertjes and Sperling [6].

III. Nonlinear Model Validation by Frequency-Domain Measurements

The efficient and accurate access to linear model validation and estimation via frequency-domain measurements provides the main motivation for adopting a similar approach to perform a nonlinear systems analysis through such measurements. For the system at hand, a combined describing function and swept-

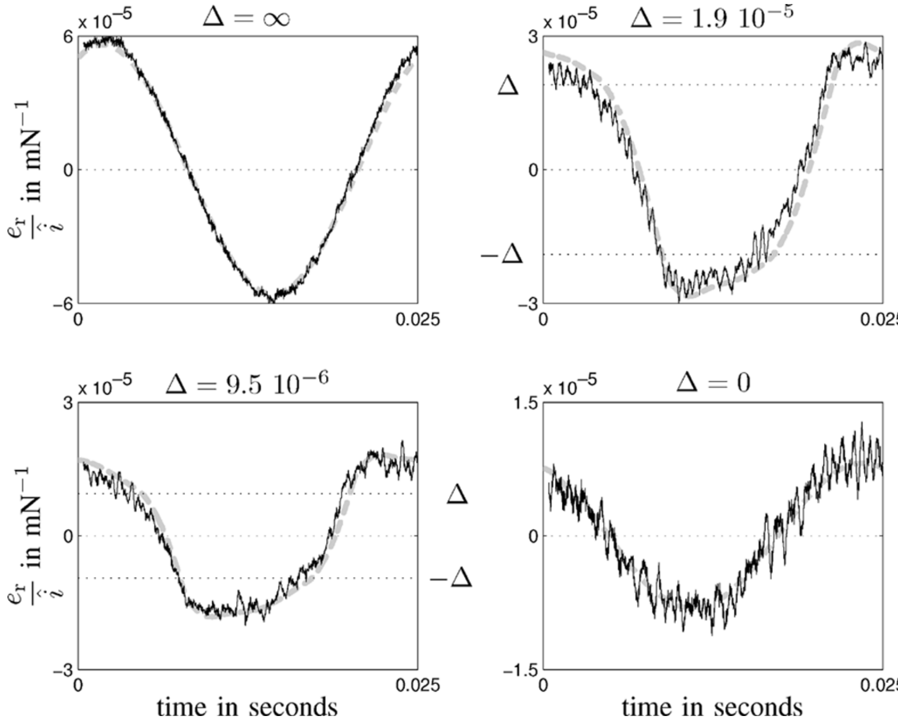

Fig. 7. Time-series under 40-Hz force excitation at different values of $\Delta = \delta/\hat{\imath}$; measured response (solid) versus simulated response (dashed).

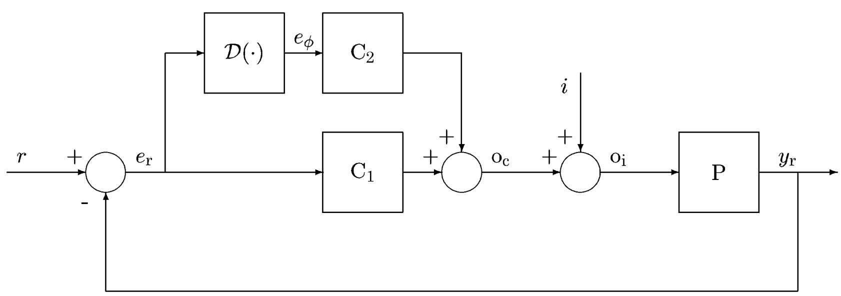

Fig. 8. Nonlinear PID controlled objective lens dynamics with describing function $\mathcal{D}$.

sine frequency-domain approach is proposed. First, however, a time-domain validation is performed based on the closed-loop nonlinear model. Second, the describing function is introduced along with the necessary validation steps. Third, the combined describing function and swept-sine measurement approach is used to assess in frequency domain both the nonlinear controller and open-loop characteristics under different vibration levels.

A time-domain validation of the nonlinear responses is shown in Fig. 7 by considering both simulations (dashed) and measurements (solid). For a fixed level of harmonic force excitation $i = \hat{\imath}\sin(\omega t)$ with $\hat{\imath} = 12.1 \times 10^{-3}$ N, an excitation frequency of 40 Hz, and four values of the scaled deadzone length $\Delta = \delta/\hat{\imath}$, it can be seen that a good agreement is obtained between forward time integration simulations and discrete-time experimental implementation. Note that the signal-to-noise ratio deteriorates for smaller values of Δ due to increased (low-frequency) disturbance rejection properties. Note, moreover, the clear presence of the fundamental frequency contribution (at 40 Hz) in the nonlinear system response. This fact, together with the computational efficiency, hence avoiding long integration times, provides the main motivation for the application of the describing function analysis to effectively approximate such responses on a model level.

In the describing function analysis, the nonlinear gain $\phi(e_\mathrm{r})$, see (5), is replaced by an approximation $\mathcal{D}(e_\mathrm{r})$ that satisfies the following relation:

$$e_\phi = \mathcal{D}(e_\mathrm{r})e_\mathrm{r}. \tag{9}$$

That is, it imposes a linear relation between a harmonic input $e_\mathrm{r} = \hat{e_\mathrm{r}}\sin(\omega t)$ and a harmonic output $e_\phi = \hat{e_\phi}\sin(\omega t)$ via the describing function $\mathcal{D}(e_\mathrm{r})$, with

$$\mathcal{D}(e_\mathrm{r}) = \Re\left\{\frac{2\alpha}{\pi}\left(\frac{\pi}{2} - \arcsin\left(\frac{\delta}{\hat{e_\mathrm{r}}}\right) - \frac{\delta}{\hat{e_\mathrm{r}}}\sqrt{1 - \left(\frac{\delta}{\hat{e_\mathrm{r}}}\right)^2}\right)\right\}. \tag{10}$$

This is standard describing function theory applied to a deadzone nonlinearity; see [11]. It is important to realize that $\mathcal{D}(e_\mathrm{r})$ depends implicitly on the frequency of excitation ω. This is due to the dependency of $\mathcal{D}(e_\mathrm{r})$ on the dimensionless ratio $\delta/\hat{e_\mathrm{r}}$ where $\hat{e_\mathrm{r}}$ implicitly depends on ω. In block-diagram representation, the nonlinear PID controlled dynamics with the describing function approximation are represented in Fig. 8. In comparing

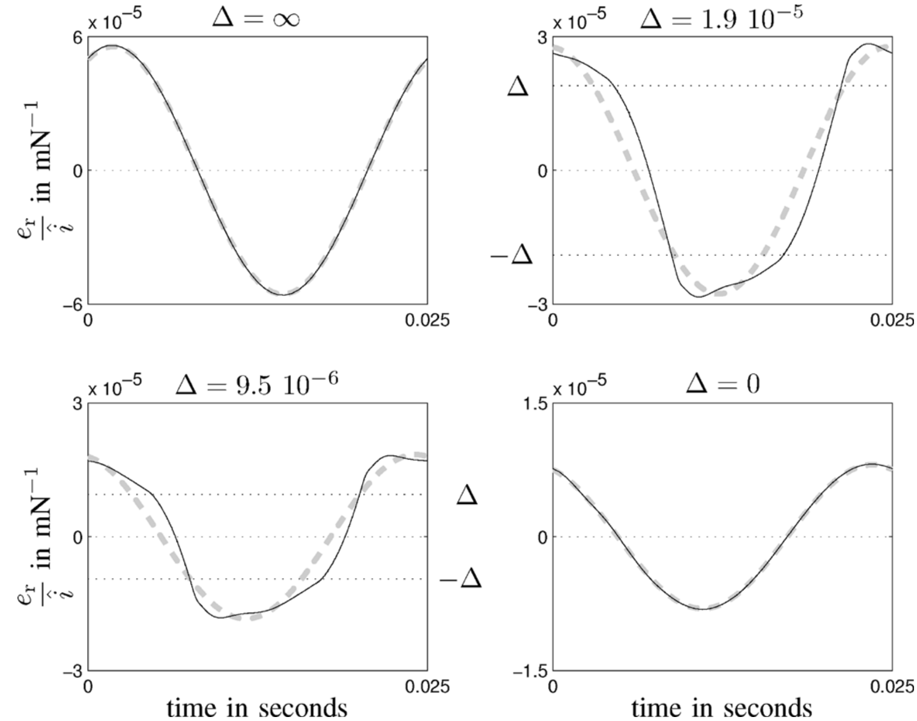

Fig. 9. Simulated time-series under 40-Hz force excitation at different values of $\Delta = \delta/\hat{\imath}$; nonlinear response (solid) versus describing function response (dashed).

this figure with Fig. 8, it can be seen that the nonlinear gain ϕ is replaced by the describing function $\mathcal{D}(\cdot)$.

Under the previously considered harmonic force input at 40 Hz with fixed amplitude of excitation $\hat{\imath}$, the responses approximated by the describing function can now be compared with the responses obtained from the full nonlinear equations of motion. Such a comparison is shown in Fig. 9 for varying values of the deadzone length $\Delta = \delta/\hat{\imath}$. It can be seen that the describing function responses very accurately describe the responses corresponding to the linear limit values of the nonlinear control design, i.e., $\Delta = 0$ and $\Delta = \infty$. For the remaining nonlinear responses, it can be seen that both the amplitude and the phase of the nonlinear responses are approximated quite well. The former property is important because of its relation with performance in optical storage drives. Hence the radial error amplitude is mainly limited by the level $e_{\mathrm{r,max}} = 0.4\ \mu$m, i.e., a quarter of the track pitch.

By comparison of Fig. 9 with Fig. 7, it is concluded that the measured nonlinear amplitudes can be accurately approximated by describing function analysis based on a single harmonic contribution. This not only justifies the application of a numerical frequency-domain performance approach based on describing function analysis but also forms the basis for the effective use of swept-sine measurements to assess the performance in experiments. That is, a quasi-steady-state analysis is obtained from (slowly) step-wise increasing the frequency of excitation. Herein user-defined frequency points are stored in a sequence of monotonically increasing values. Each sequence is evaluated for a fixed setting of the system parameters and given a fixed level of excitation. For each frequency point, the time needed for frequency response measurement is chosen sufficiently large to ensure quasi-steady-state behavior. Under quasi-steady-state conditions, the frequency response between sinusoidal input and sinusoidal output is determined at each of the frequency points sequentially.

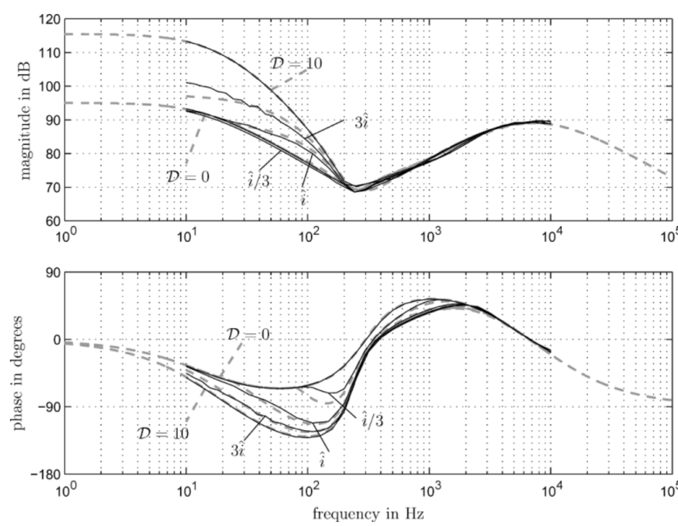

Fig. 10. Bode diagrams of the nonlinear controller frequency response functions $\mathrm{C}(j\omega)$; measured response (solid) versus simulated response (dashed).

In a combined frequency-domain approach, the outcome of the swept-sine measurement analysis is compared with the numerical results obtained from the describing function analysis. The effectiveness of such approach is demonstrated by assessing the nonlinear controller contributions under different levels of excitation. Herein the controller transfer function is given by

$$\mathrm{C}(s) = \frac{\mathrm{o_c}}{e_\mathrm{r}}(s) = \mathrm{C}_1(s) + \mathcal{D}(\cdot)\mathrm{C}_2(s) \tag{11}$$

(see also Fig. 8). Its frequency-domain behavior is depicted in Fig. 10 in Bode representation.

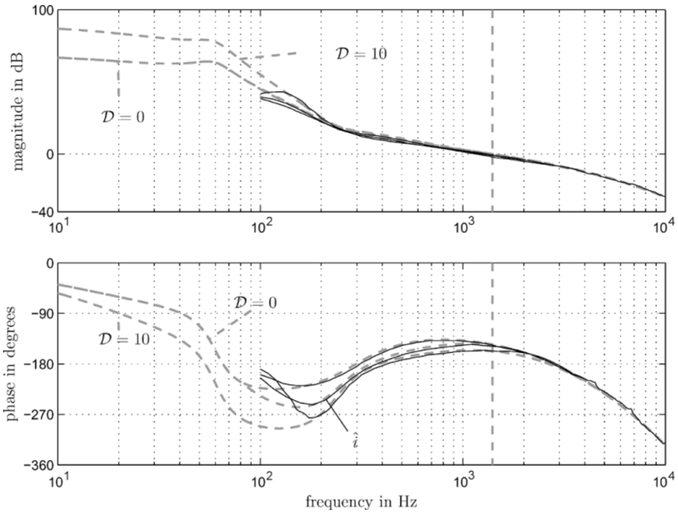

Fig. 11. Bode diagrams of the open-loop frequency response functions OL $(j\omega)$; both measured (solid) and simulated (dashed).

For the limit cases $\mathcal{D} = 0$ and $\mathcal{D} = 10$, corresponding to $\phi = 0$ and $\phi = 10$, respectively, it can be seen that a good correspondence is obtained between discrete-time measurements (solid) and simulations (dashed); note that $\mathcal{D} = 10$ implies $\phi = \alpha = 10$. The difference between $\mathcal{D} = 0$, hence $\alpha = \infty$, and $\mathcal{D} = 10$ is mainly expressed in the low-frequency range. For $\mathcal{D} = 10$, the controller induces approximately 21 dB of additional control effort, i.e., $20\log(\alpha+1)$. Apart from these linear limit cases, the characteristics for three different levels of disturbance $\hat{\imath}/3$, $\hat{\imath}$, and $3\hat{\imath}$ are depicted with $\hat{\imath} = 2.6 \times 10^{-3}$ N; the deadzone length equals $\delta = 1.0\ 10^{-7} \times$ m. These curves clearly demonstrate the shock dependency of the controller design: large shocks and vibrations induce additional control effort. For the curve labeled with $3\hat{\imath}$, the deviation between measurements and simulations below 20 Hz is caused by the poor signal-to-noise ratio that results from the closed-loop disturbance rejection properties. As a consequence, noise triggers the nonlinear gain contribution. This induces more controller effort than can be expected from the simulations in the absence of noise, hence the measured curve bends to the curve corresponding to the high-gain linear controller limit labeled with $\mathcal{D} = 10$.

Apart from the controller characteristics, the combined numerical/experimental frequency-domain approach is also used to assess the nonlinear open-loop characteristics OL, which are given in transfer function notation by

$$\mathrm{OL}(s) = -\frac{\mathrm{o_c}}{\mathrm{o_i}}(s) = \left(\mathrm{C_1}(s) + \mathcal{D}(\cdot)\mathrm{C_2}(s)\right)\mathrm{P}(s). \tag{12}$$

In Bode representation, the corresponding frequency response functions are depicted in Fig. 11. For $\mathcal{D} = 0$ and $\mathcal{D} = 10$, a good correspondence is obtained between measurements (solid) and simulations (dashed), which, by itself, provides part of the model validation of the process P. Below 150 Hz, the measurements become of poor quality; this is because all measurements are done under closed-loop conditions, hence at low frequencies the disturbance rejection properties induce a difference of at least 60 dB between input and output amplitudes. It can be seen that the open-loop characteristics show an almost common bandwidth of 1.4 kHz. However, the phase margin drops from 35° in case $\mathcal{D} = 0$ to 23° in case $\mathcal{D} = 10$. This process continues at further increasing of the gain limit value α, which is shown in Table I by numerical computation. In contrast, the gain margin roughly remains the same. For the nonlinear case with a nominal level of disturbance $\hat{\imath} = 2.6 \times 10^{-3}$ N, the phase characteristics show the behavior such as expected from the describing function analysis. It is concluded that increasing the nonlinear gain limit value α induces additional (low-frequency) control effort but at the cost of deteriorated stability margins. Such stability margin deterioration is strongly related to the nonlinear performance especially under disc defect disturbance.

TABLE I
OPEN-LOOP STABILITY MARGINS

α	0	5	10	15	20	25
phase margin in degrees	34.5	29.2	23.2	16.5	9.8	3.4
gain margin in dB	-7.4	-7.2	-7.2	-6.9	-6.6	-5.7

IV. Nonlinear Frequency-Domain Performance Assessment

For the considered nonlinear controlled objective lens dynamics, it is demonstrated that the proposed describing function and swept-sine frequency-domain approach provides the means to effectively assess nonlinear system performance on model level and experimental level, respectively. Under shocks and vibrations, this is shown, first, by nonlinear process sensitivity analysis and, second, by dropout level measurements. Third, it is shown via the relation between reduced phase margin in nonlinear Nyquist representation and the step response behavior under black-dot disturbances.

To quantify nonlinear performance under shocks and vibrations, the radial error response e_{r} is studied under force input $i = \hat{\imath}\sin(\omega t)$. This is represented by the process sensitivity function, or

$$\mathrm{S_P}(s) = \frac{e_{\mathrm{r}}}{i}(s) = \frac{-\mathrm{P}(s)}{1 + \left(\mathrm{C_1}(s) + \mathcal{D}(\cdot)\mathrm{C_2}(s)\right)\mathrm{P}(s)} \tag{13}$$

(see the block diagram of Fig. 8).

For the limit cases $\mathcal{D} = 0$ and $\mathcal{D} = 10$, Fig. 12 shows in Bode representation the results corresponding to the describing function approximation (dashed) together with the results of swept-sine measurements (solid). A good correspondence is shown both in amplitude and in phase between measurements and simulations. Differences like the high-gain mismatch near 1 kHz leave room for model improvement. For two different levels of excitation, $\hat{\imath}$ and $3\hat{\imath}$ with $\hat{\imath} = 2.6 \times 10^{-3}$N, the amplitude characteristics under nonlinear control (with $\alpha = 10$) clearly illustrate the shock-dependent behavior of the nonlinear control design. Herein the amplitude and phase characteristics demonstrate the transition from the low-gain ($\mathcal{D} = 0$) toward the high-gain limit ($\mathcal{D} = 10$). In terms of shock suppression, up to 21 dB of additional (low-frequency) improvement is demonstrated. It should be noted that the measurements are optimized for large inputs. That is, the excitation force amplitude is chosen as large as possible to improve the signal-to-noise ratio; herein the deadzone

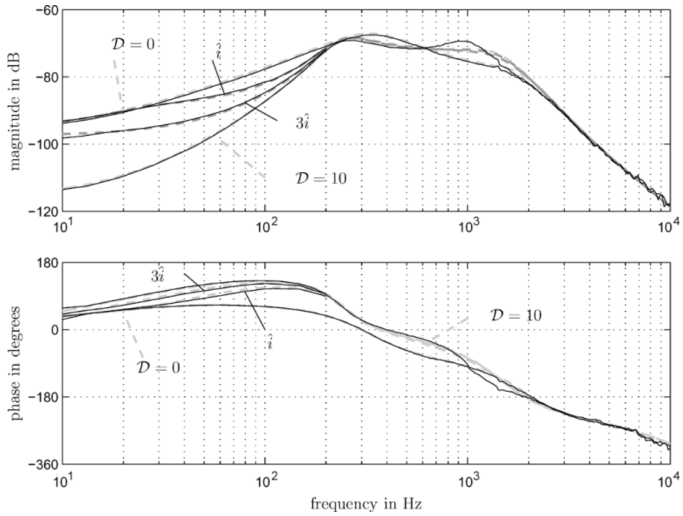

Fig. 12. Nonlinear process sensitivity frequency response functions $\mathrm{S_p}(j\omega)$; measurements (solid) and simulations (dashed) with $\alpha = 10$.

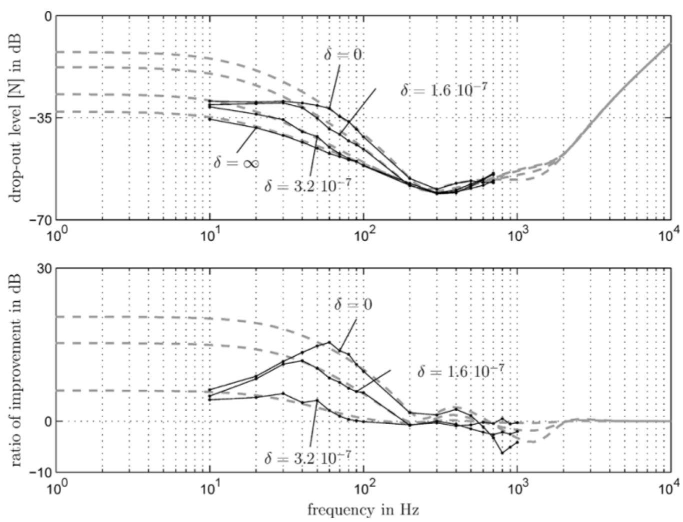

Fig. 13. Dropout level analysis; time-domain measurements (solid) versus frequency-domain simulations (dashed) with $\alpha = 10$.

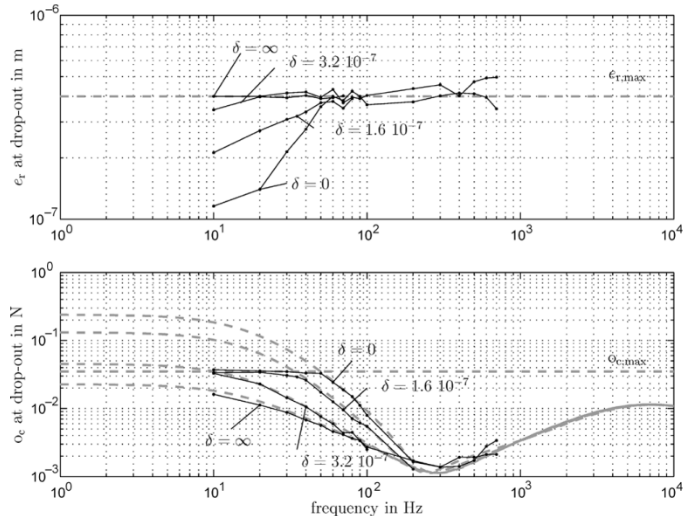

Fig. 14. Dropout level performance limitations in the radial error level $e_{\mathrm{r,max}}$ (upper part) or the controller output level $\mathrm{o_{c,max}}$ (lower part); time-domain measurements (solid) versus frequency-domain simulations (dashed) with $\alpha = 10$.

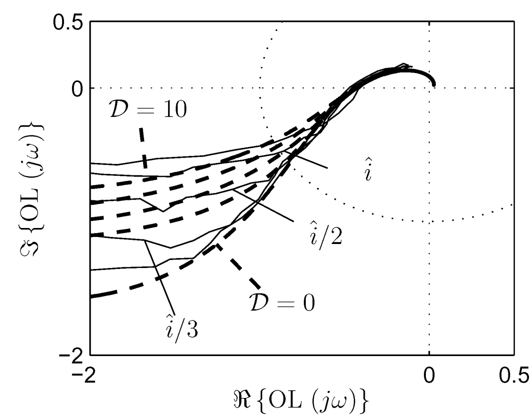

Fig. 15. Nonlinear Nyquist analysis of the open-loop frequency response function; measurements (solid) and simulations (dashed) with $\alpha = 10$.

length is scaled accordingly as to maintain comparable amplitude dependency.

Apart from process sensitivity analysis, industry often considers time-domain dropout level measurements as a means to quantify shock performance. Herein the dropout level refers to the maximum amplitude of sinusoidal disturbance at which the system at a single frequency of excitation drops out of operation. For the considered CD drive, the results of such an analysis are depicted in Fig. 13. In the upper part, the dropout level is shown under four fixed levels of the deadzone length $\delta \in \{0, 1.6 \times 10^{-7}, 3.2 \times 10^{-7}, \infty\}$ in meters. Below the level of -25 dB, it can be seen that a good correspondence is obtained between frequency-domain simulations (dashed) and time-domain measurements (solid). Herein the simulation results represent the magnitudes obtained from the frequency response function based on the describing function approximation

$$\frac{e_{\mathrm{r,max}}\left(1 + (\mathrm{C_1}(j\omega) + \mathcal{D}(e_{\mathrm{r,max}})\mathrm{C_2}(j\omega))\,\mathrm{P}(j\omega)\right)}{-\mathrm{P}(j\omega)}. \quad (14)$$

Apart from the constant $e_{\mathrm{r,max}}$, this is the reciprocal process sensitivity function evaluated at the maximum allowable radial error level $e_{\mathrm{r,max}} = 0.4\ \mu$m; see also Fig. 2 to see that this equals a quarter of the track pitch. Beyond the level of -25 dB, the controller output $\mathrm{o_c}$ saturates, giving limited shock suppression improvement. This can be seen in the lower part of Fig. 13, where the ratio of improvement relative to the low-gain linear limit ($\delta = \infty$ or $\mathcal{D} = 0$) is depicted for the levels of $\delta \in \{0, 1.6 \times 10^{-7}, 3.2 \times 10^{-7}\}$ in meters. Due to saturation, the expected low-frequency improvement of 11 times the level corresponding to the nominal linear control design is restricted to a maximum of six times obtained near 50 Hz.

For the application at hand, performance in terms of dropout is constrained by two saturation levels: 1) the radial error level $e_{\mathrm{r,max}}$ and 2) the controller output level $\mathrm{o_{c,max}}$. For the radial error, this is shown in the upper part of Fig. 14 by depicting the measured radial error amplitudes near dropout. Beyond 50 Hz, it can be seen that the radial error amplitudes do not exceed a quarter of the track pitch length, or $e_{\mathrm{r,max}}$. Below 50 Hz, these amplitudes become significantly smaller than $e_{\mathrm{r,max}}$, at least for the levels of $\delta \in \{0, 1.6 \times 10^{-7}\}$ in meters. Hence, the

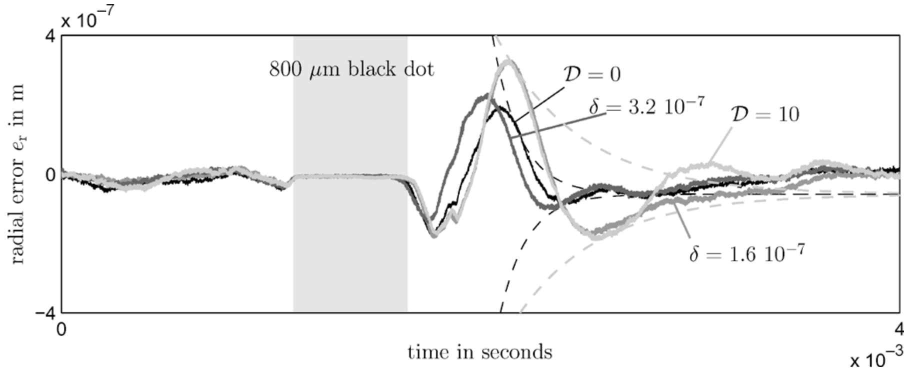

Fig. 16. Time responses under black-dot disturbances.

radial error levels are no longer solely responsible for dropout, which is now also due to saturation in the controller output o_c; saturation in the controller output induces higher harmonics for which the controlled system at the given level of excitation is too sensitive. This is clearly shown in the lower part of Fig. 14, where the measured time-domain controller output amplitudes near dropout are depicted together with the controller frequency response functions evaluated at the constant radial error level $e_{r,\max}$, or

$$e_{r,\max}\left(C_1(j\omega) + \mathcal{D}(e_{r,\max})C_2(j\omega)\right). \tag{15}$$

It can be seen that below 50 Hz, the amplitudes are restricted by the level $o_{c,\max} = 70$ mN. At this level, o_c equals 1.6 V, which represents the maximum attainable voltage at which the integrated controller circuits operate.

In addition to shocks and vibrations, performance under disc defect disturbance, which is related to reduced phase margins, can be studied using the Nyquist representation of Fig. 15. Here the open-loop frequency response functions related to (12) are depicted at three different levels of excitation, i.e., the nominal level $\hat{\imath} = 2.6 \times 10^{-3}$ N, $\hat{\imath}/2$, and $\hat{\imath}/3$. Additionally, the limit cases $\mathcal{D} = 0$ and $\mathcal{D} = 10$ are shown. The Nyquist representation emphasizes the differences between measurements and simulations by considering both mismatches in phase as well as in the amplitude characteristics. Nevertheless, the transition from the low-gain ($\mathcal{D} = 0$) toward the high-gain ($\mathcal{D} = 10$) limit is clearly shown in terms of reduced phase margins. It should be noted that the curves correspond to sufficiently large levels of excitation, the kind of excitation that normally would induce significant additional controller effort, hence (low-frequency) shock suppression. For the given nonlinear control design, it can be seen that the gain margins remain largely unaffected; see also Table I.

In terms of performance, deteriorated phase margins cause deteriorated time responses under disc defect disturbance. This is demonstrated in experiments in Fig. 16 for an 800 μm black-dot disturbance; see Helvoirt *et al.* [8] for other types of disc defect disturbance and their characteristics. Along the black dot, light is no longer reflected from the disc surface such that the radial error signal equals zero. As a consequence, a step response can be observed beyond the black dot crossing where the radial error signal is fully restored. For $\mathcal{D} = 0$ and $\mathcal{D} = 10$, it can be seen that differences occur in terms of damped natural frequency and damping ratio. This is related to the most significant closed-loop poles $-7.7 \times 10^3 \pm 1.1 \times 10^4 j$ (for the case that $\mathcal{D} = 0$) and $-1.4 \times 10^3 \pm 4.0 \times 10^3 j$ (for the case that $\mathcal{D} = 10$), respectively, which are obtained from the objective lens model and which are represented in Fig. 16 by the corresponding exponential envelopes. The time response under nonlinear control, which is also depicted in Fig. 16, shows the combined effect of these linear time-domain characteristics. For the considered value $\delta = 3.2 \times 10^{-7}$ m, it can be seen that the response tends to the low-gain limit response corresponding to $\mathcal{D} = 0$ except for large values of the radial error signal. For $\delta = 1.6 \times 10^{-7}$ m, the response tends more to the $\mathcal{D} = 10$ case for large errors (right after the black-dot crossing). As soon as the radial error signal becomes small enough, a transition is shown toward the low-gain limit response.

In summary, the combined numerical/experimental analysis such as considered in this section is shown to be both accurate and efficient in quantifying nonlinear system performance. Based on a clear interpretation in terms of frequency response functions, it provides a necessary means to quantify the shock dependency of the nonlinear control design in the frequency domain. It also contributes to the understanding of the time-domain behavior under disc defect disturbances and allows for a clear physical interpretation of the nonlinear controller's possibilities and requirements for implementation. This supports the choice of nonlinearity in addressing both shock suppression and noise sensitivity along with its ability to enhance performance beyond the design limitations otherwise encountered under linear control.

V. Conclusions

For the purpose of model validation, estimation, and performance assessment of the considered class of nonlinear controlled systems, an efficient and accurate frequency-domain approach is presented. The approach consists of a numerical describing function method in combination with swept-sine measurements and is applied to a nonlinear controlled optical playback (CD drive) device.

The validity of the describing function approximation in assessing nonlinear system behavior is studied in the time domain. For the system at hand, a good correspondence is obtained between time-domain measurements obtained from an industrial setup and the nonlinear responses obtained from numerically solving the full nonlinear equations of motion. This clearly illustrates the validity of the simplified objective lens model. In terms of amplitudes and phases, the simulated nonlinear responses subsequently show a good correspondence with the approximative harmonic responses obtained from the describing function analysis.

In the frequency domain, nonlinear controller and open-loop frequency response functions together with nonlinear process sensitivities are measured under different levels of excitation and compared with describing function-based simulations. The results show a good correspondence between measurements and simulations, which, subsequently, indicates a proper controller implementation. The shock dependency of the control design is demonstrated along with the corresponding deterioration of phase margins and its relation to deteriorated time responses under black-dot disturbances. The results indicate up to 21 dB of potentially improved (low-frequency) shock suppression which is balanced by a phase margin reduction from 35° to 23°.

The effectiveness of the considered frequency-domain approach is given by the possibility to access both amplitude and phase characteristics under different nonlinear settings in a time-efficient manner. This allows for both analysis and fingerprinting of the nonlinear system behavior. In case of dropout level measurement analysis, this leads to the conclusion that performance is limited either by a maximum radial error level of a quarter of the track pitch, hence a physical limitation, or by saturation in the controller output level, hence a limitation in the current controller implementation.

REFERENCES

[1] B. Armstrong, D. Neevel, and T. Kusid, "New results in NPID control: tracking, integral control, friction compensation and experimental results," *IEEE Trans. Contr. Syst. Technol.*, vol. 9, no. 2, pp. 399–406, Mar. 2001.

[2] S. Bittanti, F. Dell'Orto, A. Di Carlo, and S. M. Savaresi, "Notch filtering and multirate control for radial tracking in high-speed DVD-players," *IEEE Trans. Consum. Electron.*, vol. 48, no. 1, pp. 56–62, Feb. 2002.

[3] R. W. Brockett, "The status of stability theory for deterministic systems," *IEEE Trans. Autom. Control*, vol. AC-11, no. 3, pp. 596–606, Jul. 1966.

[4] J. Freudenberg, R. Middleton, and A. Stefanopoulou, "A survey of inherent design limitations," in *Proc. Amer. Control Conf.*, Chicago, IL, 2000, pp. 2987–3001.

[5] V. Fromion and G. Scorletti, "Performance and robustness analysis of nonlinear closed-loop systems using μ_{nl} analysis: Applications to nonlinear PI controllers," in *Proc. 41st IEEE Conf. Decision Control*, Las Vegas, NV, 2002, pp. 2480–2485.

[6] M. F. Heertjes and F. B. Sperling, "A nonlinear dynamic filter to improve disturbance rejection in optical storage drives," in *Proc. 42nd Conf. Decision Control*, Maui, HI, 2003, pp. 3426–3430.

[7] M. F. Heertjes and M. Steinbuch, "Stability and performance of a variable gain controller with application to a DVD storage drive," *Automatica*, vol. 40, pp. 591–602, 2004.

[8] J. van Helvoirt, G. A. L. Leenknegt, M. Steinbuch, and H. J. Goossens, "Classifying disc defects in optical disc drives by using time-series clustering," in *Proc. Amer. Control Conf.*, Boston, MA, 2004, pp. 3100–3105.

[9] F. Jiang and Z. Gao, "An application of nonlinear PID control to a class of truck ABS problems," in *Proc. 40th IEEE Conf. Decision Control*, Orlando, FL, 2001, pp. 516–521.

[10] G. A. Leonov, D. V. Ponomarenko, and V. B. Smirnova, *Frequency-Domain Methods for Nonlinear Analysis—Theory and Applications*. Singapore: World Scientific, 1996.

[11] S. Sastry, *Nonlinear Systems; Analysis, Stability, and Control*. New York: Springer-Verlag, 1999.

[12] S. G. Stan, *The CD-ROM Drive; a Brief System Description*. Dordrecht, The Netherlands: Kluwer, 1998.

[13] M. Steinbuch and M. L. Norg, "Advanced motion control: An industrial perspective," *Eur. J. Contr.*, vol. 4, pp. 278–293, 1998.

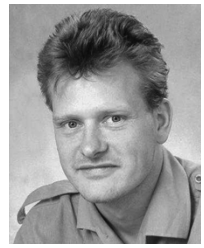

Marcel Heertjes received the M.Sc. and Ph.D. degrees in mechanical engineering from Eindhoven University of Technology, Eindhoven, The Netherlands, in 1995 and 1999, respectively.

In 2000, he joined Philips Applied Technologies, Eindhoven, where he mainly worked on nonlinear control for improved performance in optical storage drives with application to the automotive industry and active vibration isolation of metrology frames within the semiconductor industry. Since 2005, he has been subcontracted to ASML, where he works on iterative learning control of stages. He has published approximately 30 refereed papers and has received ten patents. His main focus is on the development and application of nonlinear control and dynamics in industry.

Erik Pastink was born in Amsterdam, The Netherlands, in 1978. He received the M.Sc. degree in mechanical engineering *(cum laude)* from Eindhoven University of Technology, Eindhoven, The Netherlands, in 2004.

The work for his thesis, entitled "Stability and Performance of Variable Gain Controlled Optical Storage Drives," was carried out at Philips Applied Technologies. Currently, he is a Mechatronics Design Engineer with the R&D Department, Océ Technologies, Venlo, The Netherlands.

Mr. Pastink received the Unilever Research Award in 2005 and the Royal Institution of Engineers' Control Award in 2005.

Nathan van de Wouw received the M.Sc. and Ph.D. degrees in mechanical engineering from Eindhoven University of Technology, Eindhoven, The Netherlands, in 1994 and 1999, respectively.

He joined the Philips Centre for Industrial Technology, The Netherlands, in 2000 and the Netherlands Organization for Applied Scientific Research in 2001. In 1999 he joined the Dynamics and Control group of the Department of Mechanical Engineering, Eindhoven University of Technology, as an Assistant Professor. His current research interests are the dynamics and control of nonsmooth systems.

Henk Nijmeijer (F'99) received the M.Sc. and Ph.D. degrees in mathematics from the University of Groningen, Groningen, The Netherlands, in 1979 and 1983, respectively.

From 1983 to 2000, he was with the Department of Applied Mathematics, University of Twente, Enschede, The Netherlands. Since 1997, he was also part-time with the Department of Mechanical Engineering, Eindhoven University of Technology, Eindhoven, The Netherlands. Since 2000, he has been a full Professor at Eindhoven, where he chairs the Dynamics and Control section. He has published a number of journal and conference papers and several books, including (with A. J. van der Schaft) *Nonlinear Dynamical Control Systems* (Springer-Verlag, 1990), (with A. Rodriguez) *Synchronization of Mechanical Systems* (World Scientific, 2003), and (with R. I. Leine) *Dynamics and Bifurcations of Non-Smooth Mechanical Systems* (Springer-Verlag, 2004). He is Editor-in-Chief of the *Journal of Applied Mathematics,* Corresponding Editor of the *SIAM Journal on Control and Optimization,* and a Board Member of the *International Journal of Control, Automatica, European Journal of Control, Journal of Dynamical Control Systems, SACTA, International Journal of Robust and Nonlinear Control,* and *Journal of Applied Mathematics and Computer Science.*

Prof. Nijmeijer received the Institution of Electrical Engineers Heaviside premium in 1990.